Carbon Nanotubes–Fe–Alumina Nanocomposites. Part I: Influence of the Fe Content on the Synthesis of Powders

A. Peigney, Ch. Laurent,* O. Dumortier and A. Rousset

Laboratoire de Chimie des Matériaux Inorganiques, ESA CNRS 5070, Université Paul-Sabatier, F 31062 Toulouse cedex 4, France

Abstract

Oxides based on α-alumina and containing various amounts of Fe (2, 5, 10, 15 and 20 cat%) were prepared by decomposition and calcination of the corresponding mixed-oxalates. Selective reduction of the oxides in a H_2–CH_4 atmosphere produces nanometric Fe particles which are active for the in-situ nucleation and growth of carbon nanotubes. These form bundles smaller than 100 nm in diameter and several tens of micrometers long. However, the carbon nanotubes–Fe–Al_2O_3 nanocomposite powders may also contain Fe carbide nanoparticles as well as undesirable thick, short carbon tubes and thick graphene layers covering the Fe/Fe carbide nanoparticles. The influence of the Fe content and the reduction temperature on the composition and micro/ nanostructure of the nanocomposite powders have been investigated with the aim of improving both the quantity of nanotubes and the quality of carbon, i.e. a smaller average tube diameter and/or more carbon in tubular form. A higher quantity of carbon nanotubes is obtained using α-$Al_{1.8}Fe_{0.2}O_3$ as starting compound, i.e. the maximum Fe concentration (10 cat%) allowing to retain the monophase solid solution. A further increase in Fe content provokes a phase partitioning and the formation of a Fe_2O_3-rich phase which upon reduction produces too large Fe particles. The best carbon quality is obtained with only 5 cat% Fe (α-$Al_{1.9}Fe_{0.1}O_3$), probably because the surface Fe nanoparticles formed upon reduction are a bit smaller than those formed from α-$Al_{1.8}Fe_{0.2}O_3$, thereby allowing the formation of carbon nanotubes of a smaller diameter. For a given Fe content (≤ 10 cat%), increasing the reduction temperature favours the quantity of nanotubes because of a higher CH_4 sursaturation level in the gas atmosphere, but also provokes a decrease in carbon quality. © 1998 Elsevier Science Limited. All rights reserved

1 Introduction

Since their discovery by Iijima,[1] carbon nanotubes have emerged as potentially attractive materials for the reinforcement of ceramics. Indeed, theoretical as well as experimental studies[2–7] point out that carbon nanotubes have excellent mechanical characteristics. Carbon nanotubes are commonly prepared by arc-discharge between carbon electrodes in inert gas atmosphere.[1,8] Transition metals such as iron or cobalt can be used as catalysts during the arc-discharge to increase both the quantity and length of the tubes and to favour the formation of single-shell nanotubes.[9–14] However, the so-obtained product is a mixture of carbon nanotubes and several other carbon forms, including much amorphous carbon and carbon nanoparticles. A purification has to be conducted but it decreases the nanotube yield to about 2%.[15] Recently, 'ropes' of single-wall carbon nanotubes have been obtained by an adapted laser-ablation technique.[16,17]

Other methods producing carbon filaments amongst which are some autenthic nanotubes are the catalytic decomposition of hydrocarbons,[18–22] metallocenes[23] and the disproportionation of $CO^{24–26}$ on small metal particles (Fe, Co, Ni, Cu, Mo, Pt). Several mechanisms have been proposed for the formation of tubular carbon species[26–29] by these methods, notably stressing that the metal particles are active for nanotube nucleation and growth only if they are sufficiently small (≤ 20 nm) and that the minimal tube internal diameter that

*To whom correspondence should be addressed.

can be obtained is that of the catalytic particle. In order to maximize the nanotube yield with respect to other forms of carbon, several authors investigated the influence of the temperature and of the nature of both the catalyst and the treatment atmosphere.[20,24,29,30] Dai et al.[26] have prepared single-wall carbon nanotubes ranging from 1 to 5 nm in diameter by disproportionation of CO on Mo particles a few nanometers in size. Using a zeolite-supported Co catalyst, Ivanov et al.[20] and Hernadi et al.[31] reported carbon tubes only 4 nm in diameter as well as 60 mm long tubes, but they point out that the longest tubes are also the thickest.

In previous works,[32–39] we have prepared metal–oxide nanocomposite powders by selective reduction in hydrogen of oxide solid solutions. In these materials, the metal particles (Cr, Fe, Co, Ni and their alloys) are generally smaller than 10 nm in diameter and are located both inside and at the surface of the matrix grains (Al_2O_3, Cr_2O_3, MgO, $MgAl_2O_4$). We have shown[40] that when using a H_2–CH_4 gas mixture instead of pure H_2 for the reduction of an α-$Al_{1.9}Fe_{0.1}O_3$ solid solution, the pristine Fe nanoparticles formed in situ upon reduction of the very homogeneously dispersed surface Fe^{3+} ions are active at a size adequate for the catalytic growth of nanotubes. The resulting carbon nanotubes–Fe–Al_2O_3 composite powder contains a huge amount of single- and multi-wall carbon nanotubes with a diameter in the 1·5–15 nm range. The nanotubes are arranged in bundles smaller than 100 nm in diameter and that may be up to 100 μm long. We have proposed a method based on specific surface area measurements that allows a quantification of the amount of nanotubes in the composite powder and also produces a so-called quality value, a high quality denoting a smaller average tube diameter and/or more carbon in tubular form. The total bundle length in a gram of this powder was calculated to be equal to about 100 000 km. Indeed, the metal-oxide grains are uniformly covered by a web-like network of bundles and the powder is so densely agglomerated that it retains the shape of the reduction vessel when transferred in a storage box.

In order to increase the yield in Iijima's-type nanotubes in the composite powders, it is necessary to increase the number of active catalytic particles, while avoiding their coalescence and growth on the matrix surface, and to determine the appropriate experimental conditions of the reduction step. We have first investigated[41] the influence of the crystallization level of an $Al_{1.8}Fe_{0.2}O_3$ solid solution on the formation of carbon nanotubes upon selective reduction and we have shown that it is necessary to use the stable α-$Al_{1.8}Fe_{0.2}O_3$ solid solution rather than the amorphous or η-solid solutions as starting material. Indeed, carbon is obtained essentially in the form of nanotubes in the former case, whereas important quantities of non-tubular carbon are produced in the latter cases. In addition, some carbon is entrapped within the oxide grains upon the crystallization of the amorphous or η phases in α-alumina during the reduction step. Starting from α-$Al_{1.8}Fe_{0.2}O_3$, we have also found that increasing the reduction temperature from 900 to 1000°C produces an increase in the amount of nanotubes but also a decrease in tube quality.[41]

The aim of this work is to determine the influence of the Fe content in the starting alumina-hematite compounds on the amount and quality of carbon nanotubes in the composite powders prepared by reduction at 900 or 1000°C. The micro-structure and mechanical properties of carbon nanotubes–Fe–Al_2O_3 massive materials prepared by hot-pressing these nanocomposite powders are reported in a companion paper.[42]

2 Experimental

The appropriate amounts of $(NH_4)_2(C_2O_4),2H_2O$, $Al(NO_3)_3,6H_2O$, and $Fe(NO_3)_3,9H_2O$ were mixed in an aqueous solution heated at 60°C. The obtained clear solution was cooled to room temperature and rapidly added to an alcoholic medium, in which precipitation of the mixed ammonium oxalate $(NH_4)_3[Al_{1-x}Fe_x(C_2O_4)_3],nH_2O$ ($x = 0.02$, 0·05, 0·10, 0·15, 0·20) occured immediately. After filtering, washing and oven drying, the oxalate was finely ground and decomposed at 400°C for 2 h, producing an X-ray amorphous $Al_{2-2x}Fe_{2x}O_3$ solid solution.[32,43] This oxide was calcined in air for 2 h at 1100°C and was reduced in a H_2–CH_4 gas mixture (6 mol% CH_4) during 4 h at 900°C or at 1000°C, giving rise to the carbon–metal–oxide composite powders. A total reduction of the Fe^{3+} ions present in $Al_{2-2x}Fe_{2x}O_3$ in metallic Fe would approximately yield a y wt% Fe–Al_2O_3 composite ($y = 100x$), not taking into account the presence of carbon. Thus, y stands both for the cationic content (cat%) of Fe^{3+} ions in the initial oxalate or oxide and for the weight content (wt%) of metallic phase in the composite powder, not taking into account the presence of carbon. For the sake of brevity, the composite powders will be denoted yR900 or yR1000 (2R900, 5R900, ..., 20R1000) according to their reduction temperature in the following section. The composite powders were oxidized in air at 850°C in order to eliminate all carbon, as required for the study. The powders were studied using X-ray diffraction (XRD) with Co Kα radiation ($\lambda = 0.17902$ nm) and scanning

electron microscopy (SEM). The specific surface areas of the oxide powders (S_{ss}), of the nano-composite powders obtained after reduction (S_n) and of the powders oxidized at 850°C (S_{on}) were measured by the BET method using N_2 adsorption at liquid N_2 temperature. The carbon content was determined by flash combustion.

3 Results and Discussion

3.1 Oxide powders

XRD pattern analysis showed that calcination at 1100°C of the X-ray amorphous $Al_{2-2x}Fe_{2x}O_3$ solid solutions produces monophase α-$Al_{2-2x}Fe_{2x}O_3$ (corundum) solid solutions when the Fe content is sufficiently low ($x \leq 0.10$). In contrast, the XRD patterns of specimens containing more Fe ($x = 0.15$, 0.20) present peaks characteristic of an α-Fe_2O_3-rich solid solution in addition to those of the α-Al_2O_3-rich solid solution (major phase). This traduces that some phase-partitioning occurs upon calcination in addition to crystallization, giving rise to a very intimately-mixed biphase product. These results are in agreement with earlier works.[32,43,44]

SEM observations reveal that the powders are made up of 10–20 μm agglomerates of partially sintered submicronic primary grains, showing the so-called vermicular microstructure.[45] The specific surface area measured for the calcined powders (S_{ss}) are consistent with the crystallization level revealed by XRD analysis: 5·0, 3·4, 3·1, 4·4 and 4·5 $m^2\ g^{-1}$ for the powders with $x = 0.02$, 0.05, 0.10, 0.15, 0.20, respectively.

3.2 Composite powders

3.2.1 X-ray diffraction

The XRD patterns of the nanocomposite powders prepared by reduction at 900°C of the solid solutions are shown in Fig. 1 α-Fe and Fe_3C (cementite) are detected besides corundum, the intensity of the corresponding peaks increasing with the increase in Fe content. Earlier works[32–35] have shown that the hydrogen reduction of the alumina-based solid solutions produces metallic Fe particles of nanometric size (< 10 nm), which is reflected by the relatively large width [Figs 1(b) and 1(c)] of the α-Fe (110) peak ($d_{110} = 0.203$ nm). Most of these particles are dispersed inside the grains of the Al_2O_3 matrix and therefore are thought to be protected from reacting with carbon when using a H_2–CH_4 atmosphere. However, some particles, the number of which increases with the Fe content, are located at the surface of the matrix grains and can form Fe_3C. In the case of specimens prepared from
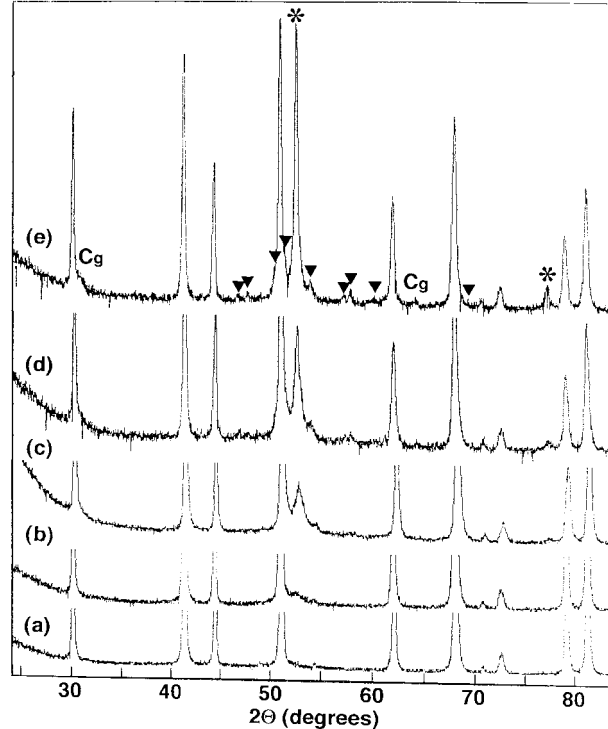
Fig. 1. XRD patterns of the nanocomposite powders prepared by reduction at 900°C: (a) 2 wt% Fe; (b) 5 wt% Fe; (c) 10 wt% Fe; (d) 15 wt% Fe; (e) 20 wt% Fe; α-Fe; ▼: Fe_3C; Cg: corresponding to d_{002} and d_{004} in multi-wall nanotubes and/or in graphite. Un-indexed peaks: α-alumina.

a mixture of an α-Al_2O_3-rich solid solution and an α-Fe_2O_3-rich solid solution (15R900 and 20R900), reduction of the latter oxide gives rise to another population of Fe particles (≥ 30 nm in size) also located on the surface of the alumina grains.[32] This is reflected by the strong increase in the α-Fe (110) peak intensity and the decrease in its width. Some of these particles may also react to form Fe_3C.

Wide peaks which could correspond to the distance between graphene layers ($d_{002} = 0.34$ nm and $d_{004} = 0.17$ nm) are also detected. Since neither the (hk0) nor the other (hkl) reflexions, which would have much smaller intensities for nanotubes as well as for graphite,[46] are detected, it is not possible from the XRD patterns to discriminate between graphite and other graphenic forms of carbon such as nanotubes. Thus we have labelled these peaks C_g ($C_{graphene}$).

A $FeAl_2O_4$ spinel phase, which is known to form at the Fe/Al_2O_3 interface upon reduction in pure H_2 at temperatures lower than 1000°C,[33,34,47,48] is not detected in the R900 powders. One cannot rule out its presence in small quantities, because the $FeAl_2O_4$ main diffraction peaks ($d_{113} = 0.245$ nm, $d_{004} = 0.202$ nm and $d_{044} = 0.143$ nm) may be masked by α-Fe and Fe carbides peaks. However, neither Fe^{3+} nor Fe^{2+} ions were detected on the room temperature Mössbauer spectrum[41] of the 10R900 composite, showing that the presence of CH_4 in the reducing atmosphere strongly favours

the formation of metallic Fe. Indeed, when reducing in pure H_2, the Fe^{3+} ions substituting for Al^{3+} ions in the solid solutions were found to be totally reduced only after a treatment at 1300°C for 5 h.[35]

Essentially similar features are observed on the XRD patterns of the nanocomposite powders prepared by reduction at 1000°C (Fig. 2), Fe_5C_2 being detected instead of Fe_3C. According to Wagman *et al.*,[49] the CH_4 equilibrium content in H_2–CH_4 gas mixtures is lower at 1000°C (ca 0·9%) than at 900°C (ca 1·9%). Thus, the CH_4 sursaturation level in the gas mixture used in the present study (6 mol% CH_4) is much higher at 1000°C (6·6 times more) than at 900°C (3·2 times more), which could account for the obtention of a higher carbide. It is noteworthy that Baker *et al.*[50] have shown that metallic Fe, and not an Fe carbide, is the active phase responsible for the formation of carbon nanofilaments. However, for a given Fe content, comparison of the α-Fe (110) peak in the R900 and R1000 powders (Figs 1 and 2, respectively) shows that it is less intense for 2 and 5R900 than for 2 and 5R1000 and that it is wider and less intense for 10 and 15R900 than for 10 and 15R1000. These results indicate that the Fe surface particles are smaller in the R900 powders than in the corresponding R1000 powders, probably owing to an easier coalescence of the metal particles at the higher reduction temperature. For the same reason, the Fe surface particles are also probably smaller in 20R900 than in 20R1000. However, one can not distinguish this so easily on the XRD patterns because the 20R900 α-Fe (110) peak is already very intense and thin.

γ-Fe may be present in all or some powders, but is extremely difficult to detect on the XRD patterns because the γ-Fe (111) diffraction peak ($d_{111} = 0.208$ nm) is probably masked by the basis of the corundum (113) peak ($d_{113} = 0.2085$ nm), the more so if Fe_3C ($d_{210} = 0.206$ nm) or Fe_5C_2 ($d_{210} = 0.208$ nm) is present as well. However, a Mössbauer spectroscopy study[41] of the 10R900 and 10R1000 composites has shown that ca 33% of the total Fe-species is in the form of γ-Fe, which could reflect the formation of a γ-Fe–C alloy rather than pure Fe.

3.2.2 Carbon content

The carbon content measured in the nanocomposite powders (C_n, Fig. 3) is in the 0·6–5·4 t% range for the R900 powders, with a maximum for 15R900. C_n is much higher for 15 and 20R900 than for the other specimens, a large gap being observed between 10 and 15 R900. For the R1000 powders, C_n is in the 2·5–6·2 wt% range, with a maximum for 10R1000, this value being significantly higher
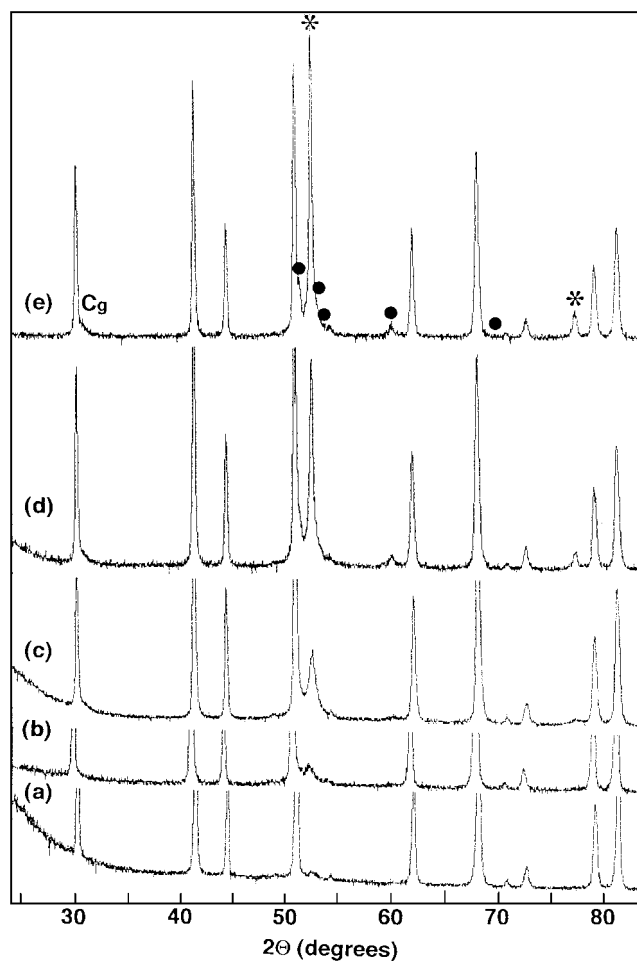

Fig. 2. XRD patterns of the nanocomposite powders prepared by reduction at 1000°C: (a) 2 wt% Fe; (b) 5 wt% Fe; (c) 10 wt% Fe; (d) 15 wt% Fe; (e) 20 wt% Fe; α-Fe; ●: Fe_5C_2; Cg: corresponding to d_{002} in multi-wall nanotubes and/or in graphite. Un-indexed peaks: α-alumina.
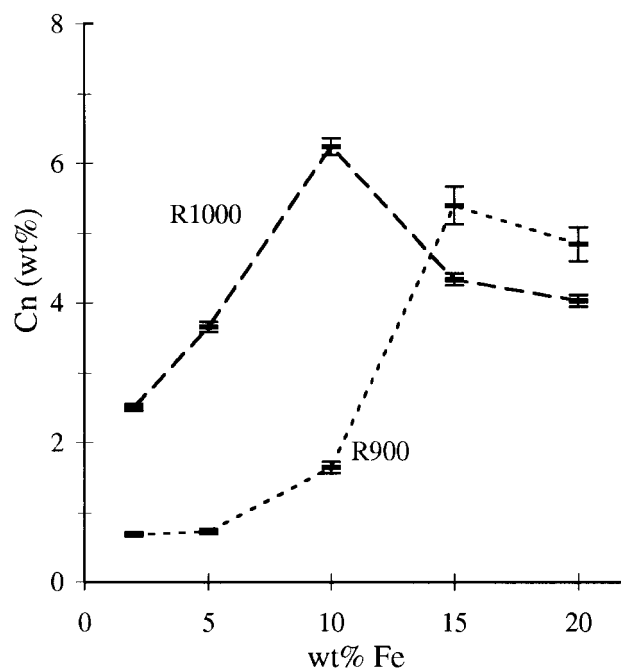

Fig. 3. The carbon content (C_n) versus the Fe content in the nanocomposite powders.

than for the other R1000 powders. For a given reduction temperature, the maximum corresponds to the Fe content that most favours CH_4 decomposition in the present experimental condition, which could be related to the high number and the relatively small size of catalytic particles. Observing a decrease in C_n for the higher metal contents (20R900 in one series, 15 and 20R1000 in the other) thus denotes that the surface particles in these specimens are less active for the catalytic decomposition of CH_4, probably because they are much larger than in the other powders as shown by the XRD results. This could also explain why C_n is lower for 15R1000 and 20R1000 than for 15R900 and 20R900. On the contrary, it is noteworthy that C_n is significantly higher for 2, 5 and 10R1000 than for 2, 5 and 10R900. This will be discussed later in this paper.

3.2.3 Scanning electron microscopy
In line with earlier results,[40,41] SEM observations of the composite powders showed that the matrix grains, forming agglomerates ca 20 μm large, are covered by a web-like network of carbon filaments not larger than 100 nm in diameter and several tens of micrometers long (Fig. 4). Note that owing to metallization the filaments appear slightly larger than they actually are. This web-like network allows the reduced powders to generally retain the shape of the reduction vessel when transferred in a storage box. TEM observations[40,41] have evidenced that these long filaments are bundles of Iijima's-type carbon nanotubes and that the surface Fe or Fe carbide particles are covered by a few graphene layers. Much fewer filaments, with much smaller diameters, are detected in the 2R900 and 2R1000 powders [Fig. 4(a)] than in the other powders. This is reflected by a lower agglomeration state of these 2 wt% Fe powders. But for all the other powders, SEM images do not allow to determine the difference in filament quantity with respect to the Fe content or the reduction temperature. In the 5 wt% Fe powders, most filaments have a diameter smaller than a few tens of nanometers [Fig. 4(b)], but some larger bundles looking like ribbons which are sometimes twisted to form buckles are also locally observed [Figs 4(c) and (d)]. The network of filaments on a porous matrix grain is clearly seen on the next image [10R900, Fig. 4(e)] and a low incidence image [10R1000, Fig. 4(f)] shows the extensive buckling of filaments at the surface of a matrix grain, demonstrating the high flexibility of carbon nanotubes and carbon nanotube bundles, as reported by many researchers.[2–7] The 15 and 20 wt% Fe powders differ from the other ones on two points: the presence of a higher proportion of large ribbon-like bundles [15R900, Fig. 4(g)] and

that of some irregularly shaped filaments of large diameter and small length [20R900, Fig. 4(g)]. These large filaments [pointed by arrows in Fig. 4(h)] seem to be tubes containing a core probably made of Fe or Fe carbide.[41]

3.2.4 Specific surface area
As proposed elsewhere,[40,41] the difference $\Delta S = S_n - S_{on}$ between the specific surface area of the nanocomposite powder (S_n) and that of the same powder after oxidation in air at 850°C (S_{on}) essentially represents the quantity of nanotube bundles in the composite powder. ΔS is plotted versus the Fe content both for the R900 and R1000 composites in Fig. 5. The values are in the $1\cdot2$–$2\cdot6$ m^2 g^{-1} range for the R900 powders and in the $0\cdot7$–5 m^2 g^{-1} range for the R1000 specimens. Both curves present a maximum for 10 wt% Fe. The evolution of ΔS with Fe concentration is similar to that of the carbon content C_n (Fig. 3) except for 15R900 and 20R900, which contain much more carbon than 10R900 but present a lower ΔS. Also, a C_n higher for 2R1000 than for 2R900 is not reflected by a higher ΔS. Interestingly, ΔS for 5R1000 and 10R1000 are significantly higher than for the other powders.

Calculations of $\Delta S/C_n$ may help to get a better understanding of the nature of the powders and explain some of the observed discrepancies. Indeed, the increase in specific surface area by gram of carbon, $\Delta S/C_n$, can be considered as representing the quality of the nanotubes, a higher figure for $\Delta S/C_n$ denoting a smaller average tube diameter and/or more carbon in tubular form,[40,41] which we consider a better quality of carbon. $\Delta S/C_n$ is plotted versus the Fe content both for the R900 and R1000 composites in Fig. 6. The values are in the 25–250 m^2 g^{-1} range for the R900 powders but only in the 20–100 m^2 g^{-1} range for the R1000 specimens, with a maximum for 5 wt% Fe on both curves. It is noteworthy that the higher $\Delta S/C_n$ are found in specimens (2, 5 and 10 R900) with a relatively low ΔS (Fig. 5) and thus that the increase in nanotube quantity observed in some powders (5 and 10R1000) upon the increase in reduction temperature is associated with a lower quality. Furthermore, the ΔS increase from 5 to 10 cat% Fe in both series is also connected to a significant decrease in quality. However, $\Delta S/C_n$ for the 15 and 20 wt% Fe powders are similar whatever the reduction temperature.

3.2.5 Discussion
For a given reduction temperature, when the nanocomposite powders are prepared by reduction of a monophase α–$Al_{2-2x}Fe_{2x}O_3$ solid solution, as is the case for specimens containing 2, 5 and
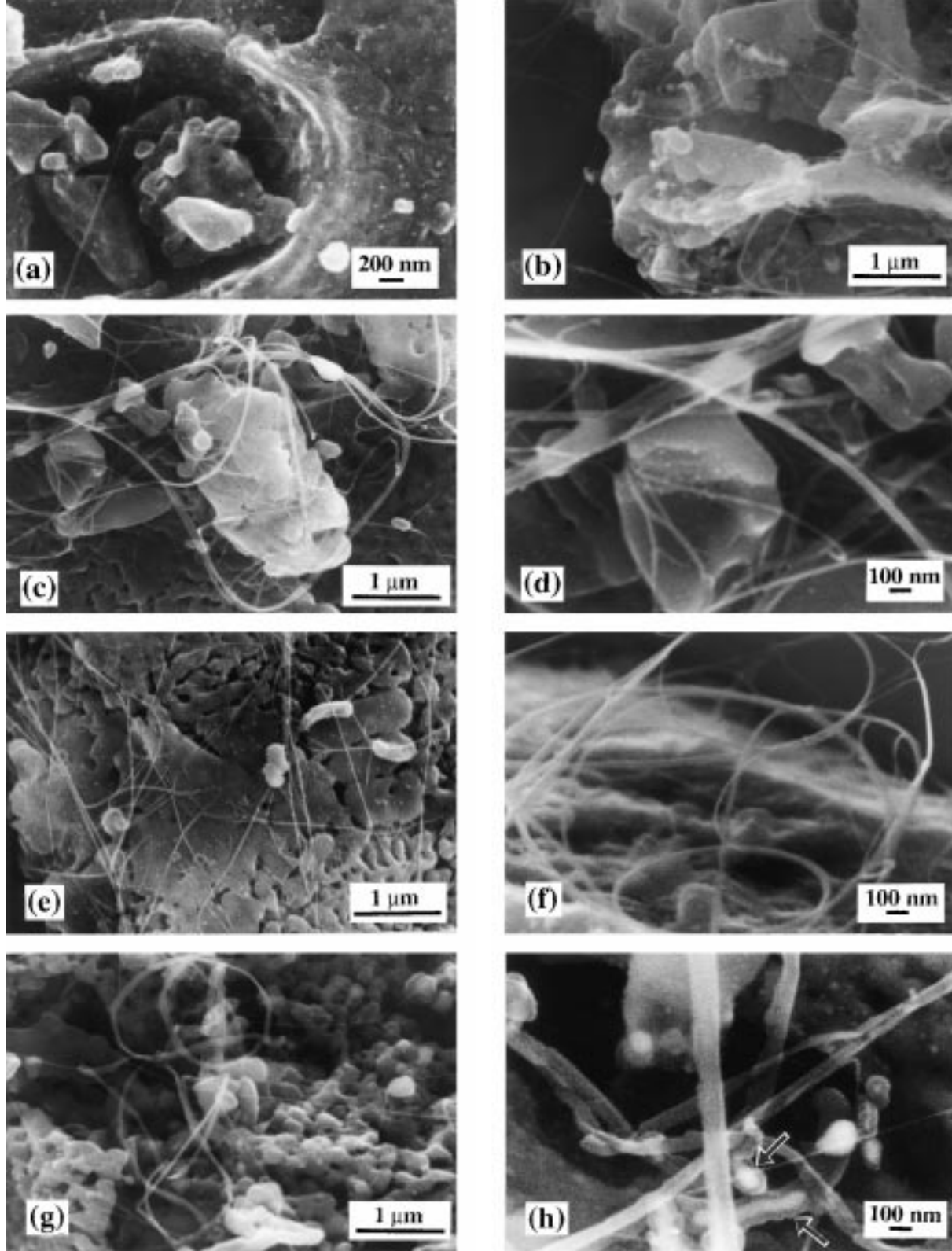
Fig. 4. SEM images of the nanocomposite powders: (a) 2R1000; (b) 5R1000; (c) 5R900; (d) higher magnification of (c); (e) 10R900; (f) 10R1000; (g) 15R900; (h) 20R900.

10 wt% Fe, the carbon content (C_n Fig. 3) and nanotube quantity (ΔS Fig. 5) increase with the Fe content. Indeed, more and more metal particles are present at the surface of the matrix grains and are available for CH_4 decomposition, nanotube nucleation and possibly nanotube growth. The

carbon nanotube quality ($\Delta S / C_n$ Fig. 6) present a maximum for the composites containing only 5 wt% Fe. Since the internal diameter of the tube is that of the corresponding catalytic metal particle, higher quality tubes are obtained when using smaller metal particles. Indeed, as shown by the
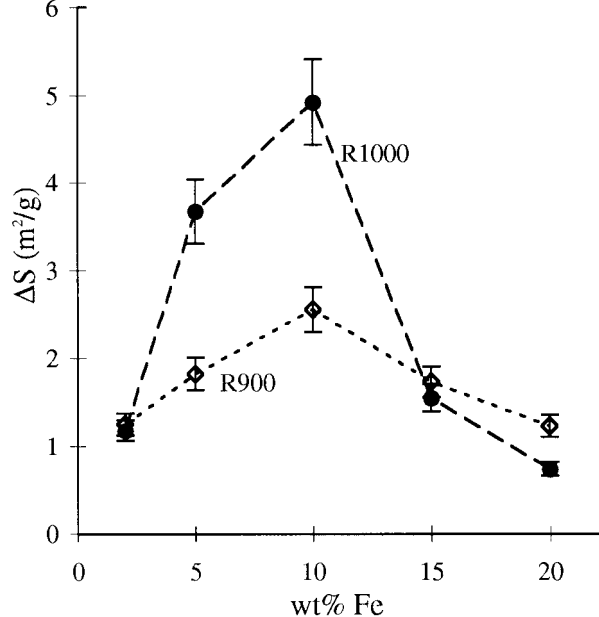
Fig. 5. $\Delta S = S_n - S_{on}$ versus the Fe content in the nanocomposite powders (S_n is the specific surface area of the nanocomposite powder and S_{on} that of the powders oxidized at 850°C).
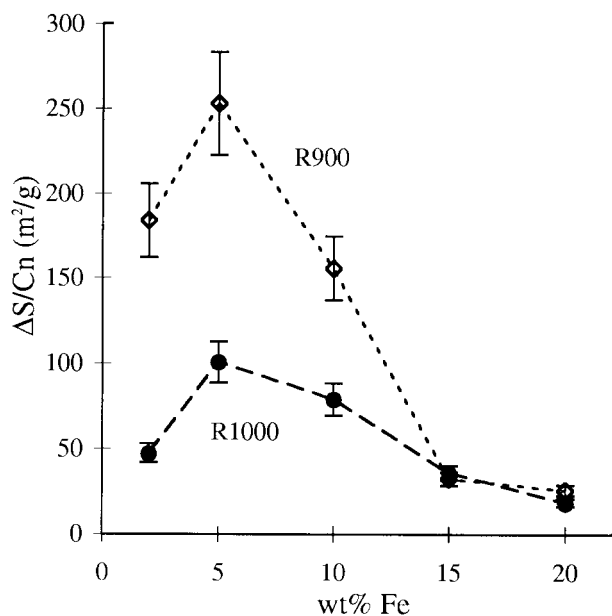
Fig. 6. $\Delta S/C_n$ versus the Fe content in the nanocomposite powders ($\Delta S = S_n - S_{on}$ where S_n is the specific surface area of the nanocomposite powder, S_{on} that of the powders oxidized at 850°C; C_n is the carbon content in the nanocomposite powder).

XRD results, the Fe surface particles are smaller for 5 wt% Fe than for 10 wt% Fe, probably because of less coalescence on the matrix surface. However, for the 2 wt% Fe powders, in which the Fe surface particles may be still more smaller, $\Delta S/C_n$ is not higher (Fig. 6). This could be explained by a larger proportion of Fe carbide particles at the grain surface, but this can not be confirmed by XRD or Mössbauer spectroscopy because of the too low Fe content.

In contrast, when the nanocomposite powders are prepared by reduction of an intimate mixture of an Al_2O_3-rich oxide and an Fe_2O_3-rich phase (15 and 20 wt% Fe powders), some differences in the C_n evolution appears (Fig. 3), depending on the reduction temperature. C_n weakly decreases from 15 to 20 wt% Fe both for R900 and R1000, but with a large gain observed for 15R900 from the 10R900 value, in contrast to the evolution between 10R1000 to 15R1000. In addition, both the quantity (ΔS Fig. 5) and quality ($\Delta S/C_n$ Fig. 6) decrease with the Fe content and are much lower than for 10 wt% Fe. In this case, the reduction of the Fe_2O_3-rich phase, which is known to be much easier than that of the Al_2O_3-rich oxide,[35] produces Fe and Fe carbide particles that are too large for the nucleation of Ijima's-type[1] nanotubes but rather appear to favour the growth of thick, short tubes as observed by SEM [Fig. 4(h)]. Moreover, Bi et al.[51] have shown that nanometric cementite particles catalyze the growth of graphene layers. Such layers have been observed in our products by previous TEM studies.[40,41] Thus, for the 15 and 20 wt% Fe powders, the low values of both ΔS and $\Delta S/C_n$ could be explained by the low specific surface area of the carbon species other than nanotubes. From 10 to 15 wt% Fe, the difference between the R900 and R1000 powders may be a consequence of the difference in size of the Fe surface particles previously deduced from the XRD results. Indeed, in 15R900 these particles are probably still small enough to allow the growth of thick and short tubes, which are very numerous and represent a large quantity of carbon in comparison with the carbon nanotubes obtained in 10R900. In contrast, in 15R1000 the catalytic particles are probably too large and much of the carbon is deposited in the form of graphene layers, in relatively small quantity because of the low surface area of the large Fe particles.

For a given Fe content, the influence of the reduction temperature (900 or at 1000°C) on the observed differences in carbon content, quantity and quality of nanotubes is twofold in the present experimental conditions. Firstly, the increase in temperature favours the reduction of the ferric ions substituting in the alumina lattice and therefore the formation of catalytic metal particles. A previous study[41] of the 10R900 and 10R1000 powders has shown that neither Fe^{3+} nor Fe^{2+} ions are detected on the room temperature Mössbauer spectra, revealing that the reduction into metallic Fe and/or Fe carbide is total in both compounds. Thus, assuming that it is the same for the 2 and 5 wt% specimens, we can infer that the number of metal particles at the surface of the matrix grains is roughly similar in both series for a given Fe content. Secondly, the increase

in reduction temperature increases the CH_4 sursaturation level in the gas atmosphere (from 3·2 to 6·6 times more), which could be beneficial for tube nucleation and growth. Indeed, with 2, 5 and 10 wt% Fe, both the carbon content (C_n, Fig. 3) and nanotube quantity (ΔS, Fig. 5) are higher for the R1000 powders than for the R900 ones, except for ΔS of 2 wt% Fe. However, the carbon quality ($\Delta S/C_n$, Fig. 6) is much lower for the R1000 powders, which points out that a higher reduction temperature, and thus a higher CH_4 sursaturation level in the present experimental conditions, also favours tube thickening and/or the deposit of much non-tubular carbon species.

For the 15 and 20 wt% Fe powders, despite the increase in the CH_4 sursaturation level in the gas atmosphere from 900 to 1000°C, both C_n (Fig. 3) and ΔS (Fig. 5) are lower for the R1000 powders than for the corresponding R900 ones. As observed by XRD, the Fe surface particles are larger in the R1000 composites and Fe_5C_2 is found in the R1000 powders instead of Fe_3C in the R900 ones. Thus, for the 20R1000 powder, as mentioned previously for 15R1000, the Fe surface particles are probably too large to even produce the thick, short tubes and they offer less surface for the deposition of the graphene layers. Fe_5C_2 surface particles may also be less catalyticaly active than Fe_3C for the growth of graphene layers. But whatever the reduction temperature, both the quantity (ΔS, Fig. 5) and quality ($\Delta S/C_n$, Fig. 6) are low because of the growth of carbon species other than nanotubes. Increasing the Fe content in the composite powder up to a value higher than 10 wt% is not beneficial with respect to the formation of nanotubes.

In agreement with previous observations,[41] the present results suggest that a compromise between a higher quantity of nanotubes and a higher carbon quality has to be found. High tube quantity is favoured by increasing the Fe content up to 10 wt% and performing the reduction at a higher temperature (1000°C), whereas less Fe (5 wt%) and a lower reduction temperature (900°C) are beneficial with respect to quality.

4 Conclusions

Oxides based on α-alumina and containing various amounts of Fe (2, 5, 10, 15 and 20 cat%) were prepared by decomposition and calcination of the corresponding mixed-oxalates. Specimens in which the Fe content is below the solubility limit of hematite in α-alumina ($\leq$10 cat% Fe) are monophase solid solutions of general formula α-$Al_{2-2x}Fe_{2x}O_3$ ($0 \leq x \leq 0·1$), whereas those containing more Fe rather consist in a very intimate mixture of an Al_2O_3-rich oxide and an Fe_2O_3-rich phase. Selective reduction of the oxides in a H_2–CH_4 atmosphere produces nanometric Fe particles which are active for the *in-situ* nucleation and growth of carbon nanotubes, which are found to be arranged in bundles smaller than 100 nm in diameter and several tens of micrometers long. However, the so-obtained carbon nanotubes–Fe–Al_2O_3 nanocomposite powders may also contain Fe carbide nanoparticles as well as undesirable thick, short carbon tubes and thick graphene layers covering the Fe/Fe carbide nanoparticles.

Whatever the reduction temperature (900 or 1000°C), it is preferable to reduce the monophase oxides rather than the mixtures with respect to the formation of Ijima's-type carbon nanotubes. The highest quantity of carbon nanotubes is obtained using α-$Al_{1.8}Fe_{0.2}O_3$ as starting compound, i.e. the maximum Fe concentration allowing to retain the monophase solid solution. A further increase in Fe content provokes the formation of a Fe_2O_3-rich phase through phase partitioning, which upon reduction produces too large Fe particles. The higher carbon quality, i.e. a smaller average tube diameter and/or more carbon in tubular form, is obtained with only 5 cat% Fe (α-$Al_{1.9}Fe_{0.1}O_3$). Indeed, the surface Fe nanoparticles formed upon reduction are probably slightly smaller, being less numerous and therefore less prone to coalescence, than those formed from α-$Al_{1.8}Fe_{0.2}O_3$, thereby allowing the formation of carbon nanotubes of a smaller diameter.

For a given Fe content, lower than 10 cat%, the increase in reduction temperature from 900 to 1000°C increases the quantity of carbon nanotubes, because the CH_4 sursaturation level in the reducing atmosphere is higher at 1000 than at 900°C. However, the simultaneous decrease in carbon quality points out that a higher reduction temperature also favours tube thickening and/or the deposit of much non-tubular carbon species in the present experimental conditions.

In agreement with previous observations,[41] the present results suggest that a compromise has to be found to favour either the quantity of nanotubes or the carbon quality. However, a detailed study of the influence of the reduction temperature, the dwell time and the composition of the reduction atmosphere could yield an improvement in both the quantity and quality of carbon nanotubes in the nanocomposite powders.

References

1. Iijima, S., Helical microtubules of graphitic carbon. *Nature*, 1991, **354**, 56–58.
2. Calvert, P., Strength in disunity. *Nature*, 1992, **357**, 365–366.

3. Ajayan, P. M., Stephan, O., Colliex, C. and Trauth, D., Aligned carbon nanotube arrays formed by cutting a polymer resin-nanotube composite. *Science*, 1994, **265**, 1212–1214.

4. Ruoff, R. S. and Lorents, D. C., Mechanical and thermal properties of carbon nanotubes. *Carbon*, 1995, **33**, 925–930.

5. Sinnott, S. B., White, C. T. and Brenner, D. W., Properties of novel fullerene tubule structures: a computational study. *Mat. Res. Soc. Symp. Proc.*, 1995, **359**, 241–246.

6. Iijima, S., Brabec, C., Maiti, A. and Bernholc, J., Structural flexibility of carbon nanotubes. *J. Phys. Chem.*, 1996, **104**, 2089–2092.

7. Treacy, M. M. J., Ebbesen, T. W. and Gibson, J. M., Exceptionally high Young's modulus observed for individual carbon nanotubes. *Nature*, 1996, **381**, 678–680.

8. Ebbesen, T. W. and Ajayan, P. M., Large-scale synthesis of carbon nanotubes. *Nature*, 1992, **358**, 220–222.

9. Iijima, S. and Ichihashi, T., Single-shell carbon nanotubes of 1 nm diameter. *Nature*, 1992, **363**, 603–605.

10. Bethune, D. S., Kiang, C. H., de Vries, M. S., Gorman, G., Savoy, R., Vazquez, J. and Beyers, R., Cobalt-catalysed growth of carbon nanotubes with single-atomic-layer walls. *Nature*, 1993, **363**, 605–607.

11. Kiang, C. H., Goddard, W. A., Beyers, R., Salem, J. R. and Bethune, D., Catalytic effects of heavy metals on the growth of carbon nanotubes and nanoparticles. *J. Phys. Chem. Solids*, 1996, **57**, 35–39.

12. Seraphin, S. and Zhou, D., Single-walled carbon nanotubes produced at high yield by mixed catalysts. *Appl. Phys. Lett.*, 1994, **64**, 2087–2089.

13. Ebbesen, T. W., Lezec, H. J., Hiura, H., Bennett, J. W., Ghaemi, H. F. and Thio, T., Electrical conductivity of individual carbon nanotubes. *Nature*, 1996, **382**, 54–56.

14. Guerret-Piecourt, C., Le Bouar, Y., Loiseau, A. and Pascard, H., Relation between metal electronic structure and morphology of metal compounds inside carbon nanotubes. *Nature*, 1994, **372**, 761–765.

15. Tohji, K., Goto, T., Takahashi, H., Shinoda, Y., Shimizu, N., Jeyadevan, B., Matsuoka, I., Saito, Y., Kasuhka, A., Oshuna, T., Hiraga, K. and Nishina, Y., Purifying single-walled nanotubes. *Nature*, 1996, **383**, 679.

16. Thess, A., Lee, R., Nikolaev, P., Dai, H., Petit, P., Robert, J., Xu, C., Lee, Y. H., Kim, S. G., Rinzler, A. G., Colbert, D. T., Scuseria, G. E., Tomanek, D., Fisher, J. E. and Smalley, R. E., Crystalline ropes of metallic carbon nanotubes. *Science*, 1996, **273**, 483–487.

17. Witanachchi, S. and Mukherjee, P., Role of temporal delay in dual-laser ablated plumes. *J. Vac. Sci. Technol. A*, 1995, **3**, 1171–1174.

18. Yacaman, M. J., Yoshida, M. M., Rendon, L. and Santiesteban, J. G., Catalytic growth of carbon microtubules with fullerene structure. *Appl. Phys. Lett.*, 1993, **62**, 657–659.

19. Baker, R. T. K. and Rodriguez, N., Catalytic growth of carbon nanofibers and nanotubes. *Mat. Res. Soc. Symp. Proc.*, 1994, **349**, 251–256.

20. Ivanov, V., Fonseca, A., Nagy, J. B., Lucas, A., Lambin, P., Bernaerts, D. and Zhang, X. B., Catalytic production and purification of nanotubules having fullerene-scale diameters. *Carbon*, 1995, **33**, 1727–1738.

21. Hernadi, K., Fonseca, A., Nagy, J. B., Bernaerts, D., Riga, J. and Lucas, A., Catalytic synthesis and purification of carbon nanotubes. *Synthetic Metals*, 1996, **77**, 31–34.

22. Fonseca, A., Hernadi, K., Nagy, J. B., Lambin, Ph. and Lucas, A., Model structure of perfectly graphitizable coiled carbon nanotubes. *Carbon*, 1995, **33**, 1759–1775.

23. Sen, R., Govindaraj, A. and Rao, C. N. R., Carbon nanotubes by the metallocene route.. *Chem. Phys. Lett.*, 1997, **267**, 276–280 .

24. Herreyre, S. and Gadelle, P., Effect of hydrogen on the morphology of carbon deposited from the catalytic disproportionation of CO. *Carbon*, 1995, **33**, 234–237.

25. Endo, M., Takeuchi, K., Kobori, K., Takahashi, K., Kroto, H. W. and Sarkar, A., Pyrolytic carbon nanotubes from vapor-grown carbon fibers. *Carbon*, 1995, **33**, 873–881.

26. Dai, H., Rinzler, A. G., Nikolaev, P., Thess, A., Colbert, D. T. and Smalley, R. E., Single-wall nanotubes produced by metal-catalyzed disproportion of carbon monoxide. *Chem. Phys. Lett.*, 1996, **260**, 471–475.

27. Tibbetts, G. G., Why are carbon filaments tubular? *J. Crystal Growth*, 1984, **66**, 632–638.

28. Baker, R. T. K., Harris, P. S., Thomas, R. B. and Waite, R. J., Formation of filamentous carbon from iron, cobalt, cobalt and chromium catalysed decomposition of acetylene. *J. Catal.*, 1993, **30**, 86–95.

29. Amelinckx, S., Zhang, X. B., Bernaerts, D., Zhang, X. F., Ivanov, V and Nagy, J. B., A formation mechanism for catalytically grown helix-shaped graphite nanotubes. *Science*, 1994, **265**, 635–639.

30. Oberlin, A., Endo, M. and Koyama, T., Filamentous growth of carbon through benzene decomposition. *J. Crystal Growth*, 1976, **32**, 335–349.

31. Hernadi, K., Fonseca, A., Nagy, J. B., Bernaerts, D., Fudala, A. and Lucas, A. A., Catalytic synthesis of carbon nanotubes using zeolite support. *Zeolites*, 1996, **17**, 416–423.

32. Devaux, X., Laurent, Ch. and Rousset A., , Chemical synthesis of metal nanoparticles dispersed in alumina. *Nanostruct. Mater.*, 1993, **2**, 339–346.

33. Laurent, Ch., Rousset, A., Verelst, M., Kannan, K. R., Raju, A. R. and Rao, C. N. R., Reduction behaviour of Fe^{3+}/Al_2O_3 obtained from the mixed oxalate precursor and the formation of the Fe^0-Al_2O_3 metal–ceramic composite. *J. Mater. Chem.*, 1993, **3**, 513–518.

34. Verelst, M., Kannan, K. R., Subbanna, G. N., Rao, C. N. R., Laurent, Ch. and Rousset, A., Investigations of the reduction behavior of iron-impregnated alumina gels (Fe/AlOOH) and the formation of Fe^0–Al_2O_3 metal–ceramic composite.. *J. Mater. Res.*, 1992, **7**, 3072–3079.

35. Laurent, Ch., Demai, J. J., Rousset, A., Kannan, K. R. and Rao, C. N. R., Fe–Cr/Al_2O_3 metal–ceramic composites: nature and size of the metal particles formed during hydrogen reduction. *J. Mater. Res.*, 1994, **9**, 229–235.

36. Laurent, Ch., Blaszczyk, Ch., Brieu, M. and Rousset, A., Elaboration, microstructure and oxidation behavior of metal–alumina and metal–chromia nanocomposite powders. *NanoStruct. Mater.*, 1995, **6**, 317–320.

37. Quénard, O., Laurent, Ch., Brieu, M. and Rousset, A., Synthesis, microstructure and oxidation of Co–$MgAl_2O_4$ and Ni–$MgAl_2O_4$ nanocomposites powders. *NanoStruct. Mater.*, 1996, **7**, 497–507.

38. Quénard, O., De Grave, E., Laurent, Ch. and Rousset, A., Synthesis, microstructure and thermal behaviour of $Fe_{0.65}Co_{0.35}$–$MgAl_2O_4$ and $Fe_{0.65}Ni_{0.35}$–$MgAl_2O_4$ nanocomposites powders. *J. Mater. Chem.*, 1997, **7**, 2457–2467.

39. Carles, V., Brieu, M. and Rousset, A., Chemical synthesis and characterization of $Fe_{0.65}Ni_{0.35}$–MgO nanocomposite powders. *NanoStruct. Mater.*, 1997, **8**, 529–544.

40. Peigney, A., Laurent, Ch., Dobigeon, F. and Rousset, A., Carbon nanotubes grown in-situ by a novel catalytic method. *J. Mater. Res.*, 1997, **12**, 613–615.

41. Laurent, Ch., Peigney, A. and Rousset, A., Synthesis of carbon nanotubes–Fe–Al_2O_3 nanocomposite powders by selective reduction of different $Al_{1.8}Fe_{0.2}O_3$ solid solutions. *J. Mater. Chem.*, 1998, **8**, 1263–1271.

42. Laurent, Ch., Peigney, A., Dumortier, O. and Rousset, A., Carbon nanotubes–Fe–alumina nanocomposites. Part II: microstructure and mechanical properties of the hot-pressed composites. *Journal of the European Ceramic Society*, 1998, **18**(14), 2005–2013.

43. Rousset, A. and Paris, J., Formation de solutions solides binaires et ternaires des sesquioxydes de chrome, aluminium et de fer. III–Le système Fe_2O_3–Al_2O_3. *Bull. Soc. Chim. Fr.*, 1972, **10**, 3729–3733.

44. Muan, A. and Somiya, S., Phase equilibrium studies in the system iron oxide–Al_2O_3–Cr_2O_3. *J. Am. Ceram. Soc.*, 1959, **42**, 603–613.

45. Messing, G. L., McArdle, J. L. and Shelleman, R. A., The need for controlled heterogeneous nucleation in ceramic processing. *Mat. Res. Soc. Symp. Proc.*, 1986, **73**, 471–480.

46. Seshadri, R., Govindaraj, A., Aiyer, H. N., Sen, R., Subbanna, G. N., Raju, A. R. and Rao, C. N. R., Investigations of carbon nanotubes. *Current Sci.*, 1994, **66**, 839–847.

47. Marchand, A., Devaux, X., Barbara, B., Mollard, P., Brieu, M. and Rousset, A., Microstructural and magnetic characterization of alumina-iron nanocomposites. *J. Mat. Sci.*, 1993, **28**, 2217–2226.

48. Devaux, X., Laurent, Ch., Brieu, M. and Rousset, A., Iron–alumina interface in ceramic matrix nanocomposites. *J. All. Comp.*, 1992, **188**, 179–181.

49. Wagman, D. D., Kirpatrick, J. E., Taylor, W. J., Pitzer, K. S. and Rossini, F. D., Heats, free energies, and equilibrium constants of some reactions involving O_2, H_2, H_2O, C, CO, CO_2 and CH_4. *J. Res. Natl. Bur. Stand.*, 1945, **34**, 143–161.

50. Baker, R. T. K., Alonzo, J. R., Dumesic, J. A. and Yates, D. J. C., Effects of the surface state of iron on filamentous carbon formation. *J. Catal.*, 1977, **74**, 82–84.

51. Bi, X. X., Ganguly, B., Huffman, G. P., Huggins, F. E., Endo, M. and Eklund, P. C., Nanocrystalline α-Fe, Fe_3C and Fe_7C_3 produced by CO_2 laser pyrolysis. *J. Mater. Res.*, 1993, **8**, 1666–1674.